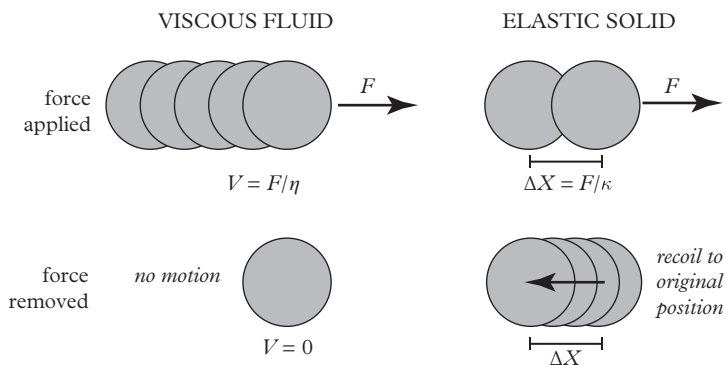# Introduction

1.1 Microrheology

Imagine mixing small magnetic particles, like iron filings, into a soft material, then turning on a nearby electromagnet, and watching the particles move. If the material is a simple, viscous liquid, the particles will slowly translate through it (see Fig. 1.1). Doubling the forcing would double the migration velocity, and turning off the forcing would stop the motion. Measuring the migration velocity V in response to a range of driving forces F would reveal a strictly linear relationship, $F = \zeta V$, where the hydrodynamic resistance ζ is specific to the properties of the particles (*e.g.*, its size and shape) and of the liquid (*e.g.*, viscosity). In analogous measurements, the same particle would move more slowly in a liquid of higher viscosity, with ζ being directly proportional to the liquid viscosity η.

If the particle is instead suspended in an elastic solid, like a soft gel, a magnetic force would cause the particle to move some distance and then stop. If the field were turned off, the particle would spring back to its original (equilibrium) position. Measuring the displacement ΔX of a particle embedded in a simple-elastic solid, in response to a series of applied forces F, would reveal a linear spring constant $F = \kappa \Delta X$. The "stiffer" the solid, the higher the spring constant κ.

We have just considered a simple microrheology experiment, not that different from the first "microrheology" experiments that date to the early-twentieth century, a body of work that parallels the nascent development of colloid science and rheology.

As early as 1922–24, researchers were reporting measurements of the mechanical properties of biological samples, including cells, by tracking the motion of embedded magnetic particles. These probes were typically iron or nickel particles, tens of micrometers in diameter, that were carefully separated from powders by mechanical screening. In one early study, Heilbronn (1922) used iron filings to measure the mechanical properties of slime molds, which consist of motile, single-cell protists of the genus *Myxomycetes*. Seifriz (1924) used nickel particles to study the viscoelasticity of sand dollar eggs, *Echinarachnius parma*, having developed these methods for experiments

VISCOUS FLUID   ELASTIC SOLID

force
applied

$V = F/\eta$ $\Delta X = F/\kappa$

Fig. 1.1 *Particle motion in viscous, Newtonian fluid and elastic solid when a force F is applied and removed.*

force
removed   *no motion*   *recoil to original position*

$V = 0$ ΔX

involving gelatin (Freundlich and Seifriz, 1923).[1] Around the same time, Heilbrunn (1924) reported measurements of clam eggs, *Cumingia tellinoides*, using a centrifuge to force endogenous granules to move through the cytoplasm.

Active and passive microrheology

Early examples of microrheology measurements highlight their essential features—to measure probe particles embedded within soft materials as they move in response to a force, and to then deduce material-response properties from that motion. In the contemporary practice of microrheology, measurements made when the force on a probe is externally imposed—like the magnetic, gravitational, or centrifugal examples provided—fall into the class of **active microrheology** techniques. The other class, called **passive microrheology**, is a more recent development, and began with the seminal work of Mason and Weitz (1995) and Gittes *et al.* (1997).

Passive microrheology employs microrheological probe particles so small—typically a micrometer or smaller—that thermal fluctuations are strong enough to drive the probe into measurable motion. Such motion arises due to the constant bombardment by surrounding molecules, which are themselves rattling around due to thermal fluctuations. A particle thus experiences random forces, exerted over many directions and strengths and over a variety of time scales. The magnitude of the forces, and how the particle responds to those random forces, depends on the material itself. A particle randomly forced within a viscous fluid will generally wander in random directions, exhibiting diffusive trajectories with mean-squared displacement[2]

$$\langle \Delta x^2(t) \rangle = 2Dt. \tag{1.1}$$

[1] Seifriz visited Herbert Freundlich, who worked in colloid chemistry and was director of the Kaiser Wilhelm Institute for Physical Chemistry and Electrochemistry from 1919 until 1933. At the time, the rheology of suspensions, especially Einstein's description of suspension viscosity, was a model for cell rheology. In this early work, the motivation to understand cell rheology didn't stem from the underlying and marvelous mechanics that arise from a microstructure of protein filaments or the action of molecular motors (see Howard (2000) and Bray (2001) to read more about the biomechanics of cells and the cytoskeleton). Early work predated our knowledge of a cell's molecular structure, genetic-heredity mechanisms, mechanics of cellular differentiation, and metabolic processes. What was clear to investigators at the time was that the rheologically *squishy* "protoplasm" of cells harbored the physical and chemical basis for life's processes. Although it appeared to be just a small, gelatinous mass, Seifriz (1928) writes, "The problem of metabolism, growth, reproduction, heredity, behavior, disease—in short, the problems of life—are the problems of the physical-chemistry of protoplasm." Presciently, Seifriz regarded the mechanics of cells as a key to understanding certain disease pathologies, including cancer.

[2] We use angle brackets $\langle . \rangle$ to denote an average taken over an ensemble in thermal equilibrium. Here, the ensemble consists of many realizations of a one-dimensional random walk, which tracks a particle's displacement X with time. See Fig. 4.20, for example.

Stokes computed the hydrodynamic resistance ζ of a sphere of radius a moving through a fluid of viscosity η (see Section 2.5.2) to be

$$\zeta = 6\pi a \eta, \qquad (1.2)$$

and Einstein (1906) and Sutherland (1905) related a particle's diffusivity D to its hydrodynamic resistance, via

$$D = \frac{k_B T}{6\pi a \eta}. \qquad (1.3)$$

The higher the viscosity, the more slowly the particle diffuses. This is the **Stokes–Einstein Relation**.[3]

A particle in an elastic solid, on the other hand, is effectively held in place as if by a spring with spring constant κ. In equilibrium, the equipartition theorem holds that the average energy stored within the spring in each of the three independent translational directions, $U = \frac{1}{2}\kappa \Delta X^2$, must be equal to $\frac{1}{2}k_B T$. The mean-square displacement will approach a constant value,

$$\langle \Delta x^2 \rangle = \frac{k_B T}{\kappa}, \qquad (1.4)$$

unlike the linear growth in time seen in a viscous liquid (eqn 1.1). The stiffer the spring, the more tightly the particle is held in place. An elasticity calculation (Section 2.5.5) relates this spring constant to the elastic constants of the material:

$$\kappa = 6\pi a G \left[\frac{6K + 8G}{6K + 11G} \right]$$
$$\approx 6\pi a G, \text{ when } K \gg G, \qquad (1.5)$$

where G is the shear modulus and K is the bulk (compressional) modulus of the material. Notably, an elastic material that is much harder to compress than shear ($K \gg G$) behaves as incompressible, with a spring constant $\kappa \approx 6\pi a G$ that looks suspiciously like Stokes drag in a liquid (eqn 1.2). This is no coincidence, as we shall see in Section 2.4.

These two limits bracket the possible responses in passive microrheology, where the forces driving the probe into motion are not imposed externally, but rather from the inherent and unquenchable thermal fluctuations within the equilibrium material. The thermal motion of small particles in a liquid or a solid, easily observed with a microscope or other means, contains a wealth of information about the properties of that material—whether viscosity, elasticity, or time scale-dependent viscoelasticity.

[3] Recently, the work of William Sutherland (1905), which paralleled Einstein's theory of Brownian motion, has been recognized. Equation 1.3 is now sometimes referred to as the Stokes–Einstein–Sutherland equation.

1.1.1   Why microrheology?

Microrheology encompasses a set of rheometric methods or techniques with unique capabilities—a part of the experimental toolbox for characterizing the rheological properties of materials to aid their understanding, or help in the design of new materials.

There are limitations to microrheology that are important to understand from the outset. Microrheology uses the movement of small particles in a material; thus, it is limited to fairly soft materials, with moduli typically no more than a few hundred pascals (not too far off from the stiffness of jello) or fluids with viscosities lower than that of honey. Many classes of materials—*e.g., polymer melts, glassy liquids, and elastomers*, for which rheological measurements played a central role in understanding—are too stiff or viscous to be amenable to microrheological methods. Despite being limited to soft materials, microrheology introduces important new capabilities for the rheologist, some of which include the following:

- **Small sample volumes**—From the studies of Heilbronn, Freundlich, and Seifriz in the early-twentieth century on, particles have been used to measure rheology in small sample volumes—down to single eukayrotic cells, with volumes ~ 1 picoliter. Particle tracking (Chapters 4 and 6), magnetic bead microrheology (Chapter 8), and laser tweezer microrheology (Chapter 9) typically require sample volumes between ~ 1 and $10~\mu$l. This sample volume makes many scarce and expensive materials available to rheological characterization, and, in particular, the ability to screen material properties over a wide range of sample conditions and compositions. Formulations of protein therapeutics and emerging biomaterials are just two examples of such samples. The small sample dimensions facilitate rapid mass and heat transfer, enabling faster screening and sample preparation and manipulation using microfluidics.

- **Short acquisition times**—Microrheology data spanning several decades in time (*e.g.,* 0.01–1 s) can be acquired by multiple particle tracking in as little as a minute. This makes it possible to track the frequency-dependent response for samples that are changing with time—during gelation or degradation, for instance. The short acquisition times also aid rapid data acquisition in screening applications, enabling tens to hundreds of samples to be processed in a single day.

- **Sensitivity**—Fluids with low viscosities and solids with small-elastic moduli are within the range of microrheology. Solutions of entangled, filamentous actin (F-actin)—a principal protein of

the cytoskeleton and muscle—appear almost Newtonian and are easily poured at 1 mg/ml concentrations in an aqueous buffer. Careful observation, however, reveals small bubbles to remain suspended, and to exhibit a subtle elastic recoil when the sample is twisted. Although its elastic modulus may be no more than one pascal, such weak moduli can reliably be measured with microrheology. More broadly, the "incipient rheology" of gel transitions in hydro- and organogelators, and the intrinsic viscosity of polymer and protein solutions, represent important and challenging classes of materials whose measurement is enabled by microrheology.

- **Extended range of frequencies**—Passive particle microrheology using diffusing wave spectroscopy (Chapter 5) or laser tracking (Chapter 6) measures probe motion on time scales as short as 1 μs, enabling high-frequency material response properties (kHz–MHz) to be measured directly, which is particularly useful when time-temperature superposition—commonly used for polymer melt rheology—is not applicable. The high-frequency response of polymer solutions and gels can be used to characterize the underlying nanometer-scale mechanics of the material—an application discussed in Section 5.6.

- **Local rheology**—Probe particles distributed throughout a sample can be used to map its spatial-rheological heterogeneity, clearly information that is not available to bulk rheology. We discuss this application in Section 4.10. With the use of multiple probe particles ("two-point microrheology," discussed in Section 4.11) the dependence of rheology as a function of length scale can be characterized.

- **Simple experiments**—Many microrheology experiments require little in the way of specialized equipment. Tracking particle motion with video microscopy is possible using only a microscope, video camera, and computer.

In short, microrheology opens a wide range of samples and conditions which may be difficult, if not impossible, to measure by conventional rheometry. Throughout the text, we will consider the **operating range** of microrheological methods to identify when they can be the greatest asset to a rheological study and to aid experimental design.[4] We also identify **application notes** in each of many of the chapters, highlighting areas where microrheology approaches to problems have been especially beneficial, and we discuss more applications in Chapter 10, including gelation and degradation of hydrogelators and biomaterials.

---

[4] The operating limits of passive microrheology are discussed in Section 3.11 and in the chapters on individual techniques. A comparison to the operating range of bulk rheology is made in Section 10.1.

Fig. 1.2 *The modulus of a peptide hydrogelator measured using laser tweezer microrheology at low concentrations and bulk rheology at higher concentrations illustrates the complementarity of the rheological measurements. Adapted with permission from Veerman, C. et al., Macromolelcules 39, 6608–14 (2006). Copyright 2006 American Chemical Society.*
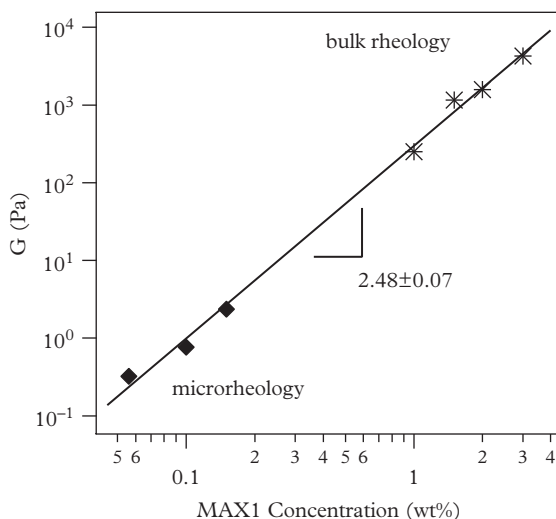
While microrheology is not a replacement for bulk rheology, one last and key benefit of microrheology is its **complementarity** to macro-rheology. The two methods can be combined to produce an understanding of a material's rheology beyond what would have been possible if only one approach were taken. This combination is illustrated by the data shown in Fig 1.2. Here, the elastic modulus of a peptide hydrogelator has been measured using oscillatory rheology and laser tweezer microrheology. The sensitivity of microrheology makes it best-suited for measurements at low peptide concentrations, when the corresponding moduli are small, whereas bulk rheology is better suited to higher concentrations and larger moduli. Together, the experiments create an interpolatable data set that spans nearly two decades in concentration and almost five decades in modulus, and is nicely consistent with the scaling with concenteration c expected for the elastic modulus of a semiflexible polymer network, $G \sim c^{5/2}$ (MacKintosh *et al.*, 1995).

The remainder of this chapter introduces background concepts that are important for microrheology, including general concepts of soft matter rheology and rheometry, rheological functions, and important aspects of colloid science.

1.2 Soft matter and rheology

The examples at the beginning of Section 1.1 described the limiting cases of particle motion in a purely viscous solvent or purely elastic

solid. Many materials of interest—especially those typically studied using microrheology—fall into a more general class of **viscoelastic** fluids and solids. The way that such materials flow and deform—even on a qualitative level—depends entirely on what is done to them. Over what time scales are forces applied? How strong are the deforming forces? Are they sheared between plates, extruded through an orifice, or pulled into fibers?

We start with brief descriptions of some common rheological phenomena exhibited by everyday materials, with the goal of highlighting the rich variety that exists. We will identify the rheological property required to describe such phenomena, then follow by describing the sorts of measurements used to characterize them.

- **Honey** is a viscous, Newtonian liquid that responds as you might expect: It flows in response to applied stresses. Double the stress, and the flow rate doubles. Here, the relevant material property is the *shear viscosity η*. Viscous liquids like honey and water are usually approximated as *incompressible*.

- A **rubber** ball bounces when dropped, and bounces even more strongly when thrown. It consists of long polymer chains, each of which behaves effectively as a molecular spring, that are crosslinked chemically to form a "permanent," three-dimensional network of attached springs. As with small-molecule elastic materials (*e.g.*, steel) the energy required to deform the material is stored elastically, then recovered when the deformation is allowed to relax—in this case, with a bounce. Rubber and other elastomers can deform much more significantly (*i.e.*, to much higher strains) than steel without changing irreversibly. As with elastic solids, the shear and compressional elastic moduli G and K are relevant, as well as stress-strain curves and failure points. Unlike molecular solids, however, the elastic moduli of elastomers depend strongly on frequency, particularly at high frequencies (short time scales). This is because the polymeric springs store more energy than small-molecule crystals; rapid stress or strain pulses stretch the polymeric springs in a non-quasi-steady (non-adiabatic) fashion, exciting only some internal degrees of freedom, which dissipate energy as they relax. Therefore, frequency-dependent viscoelastic moduli $G^*(\omega)$ are required. Because of the solid-like response over long time scales, these materials are *viscoelastic solids*. Hydrogel networks similar to the one shown in Fig. 1.3 have many of the characteristics of elastic polymer networks. The rheological characterization of hydrogels is a focus of many microrheology measurements.

Fig. 1.3 *A cryo-transmission electron micrograph showing the highly entangled and physically cross-linked network of a peptide hydrogel. The amphiphilic peptides self-assemble into semiflexible filaments to form a viscoelastic solid. Reprinted with permission from Ozbas, B., Rajagopal, K., Schneider, J. P., & Pochan, D. J. Phys. Rev. Lett. 93, 268106 (2004). Copyright 2004 by the American Physical Society.*
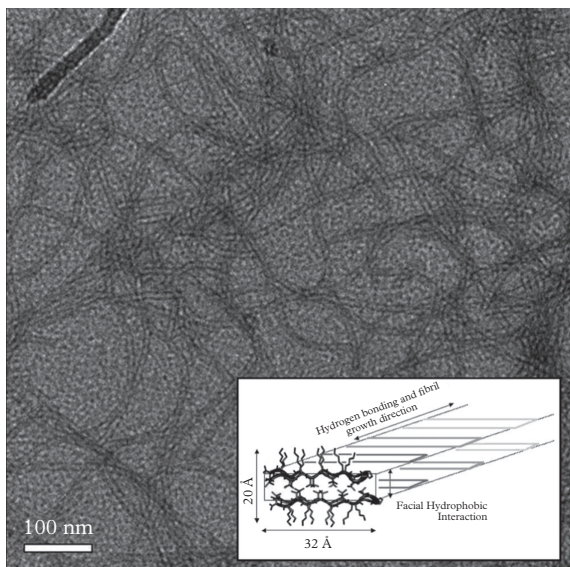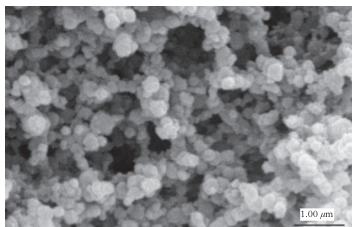
- A ball of **Silly Putty** bounces when dropped, yet spreads into a pancake when left to sit for several minutes. Like a rubber ball, a ball of Silly Putty consists of long polymer chains; yet the polymers in Silly Putty are entangled without crosslinking, constantly rearranging under thermal motion. Polymers stretch and migrate when the material is deformed, but the (temporary) entanglements that exist at any given time effectively "anchor" the molecular springs in place, much like physical or chemical cross-links. If the stress is exerted over a long enough time, the entanglements eventually relax and the material flows like a liquid. Short-lived stresses, however, do not give the entanglements time to relax, and the Silly Putty springs back like an elastic solid. Whether or not Silly Putty bounces depends entirely upon the relaxation time for the entanglements—a quantity that can be measured using small-amplitude linear rheology. As with crosslinked elastomers, frequency-dependent viscoelastic moduli $G^*(\omega)$ are required to characterize Silly Putty. At medium to high frequencies, $G^*(\omega)$ may even be identical for the two materials. At low frequencies, however, the crosslinked elastomer has a finite-shear modulus $G^*(\omega \to 0) \to G_0$, whereas the elastic shear modulus of the uncrosslinked material vanishes at low frequencies. Consequently, Silly Putty is considered to be a *viscoelastic liquid*, whereas (crosslinked) rubber balls are viscoelastic solids. The crossover frequency ω_c—below which the

elastic (real) component of $G^*(\omega_c)$ drops below the viscous (imaginary) component $G^*(\omega_c)$—is directly related to the longest relaxation time of the entanglements.

- **Mayonnaise** sits on a knife without flowing, despite the gravitational forces exerted on it. In this regard, mayonnaise appears to be a viscoelastic solid. Nonetheless, very little effort is required to spread mayonnaise on a piece of bread. Mayonnaise behaves as a solid under low stresses, but flows like a liquid above a critical *yield stress*. Mayonnaise consists of oil drops suspended in an aqueous solution at such a high concentration that drops can not move without rearranging (Fig. 1.4). Since rearrangement requires a finite amount of energy, a finite stress must be applied before it flows. Toothpaste, cake frosting, and yogurt also have yield stresses, but for different reasons: Each involves a weak, transient gel that takes some energy to break, but reforms—rapidly for frosting and toothpaste, and over longer time scales for yogurt (Fig. 1.5) Relevant rheological properties include $G^*(\omega)$, for insight into the equilibrium structure and relaxation processes, and the yield stress σ_y and yield strain γ_y.

- Watching **shampoo** flow in a bottle, one would assume it to be a liquid as viscous as honey. However, it is painless to spread shampoo into hair, whereas spreading honey into hair might pull it out. Shampoo also feels "slippery," indicating its *shear thinning* nature: It flows with high viscosity when sheared slowly, but at much lower viscosity when sheared rapidly. Shampoo shear thins because the structures that impart the high viscosity (*e.g.*, surfactant worm-like micelles) align with shear flows to facilitate the flow. The linear viscoelastic moduli $G^*(\omega)$ provide information about the structure and relaxation around equilibrium, but shear thinning requires the shear viscosity $\eta(\dot{\gamma})$ to be measured as a function of shear rate $\dot{\gamma}$.

- A drop of **saliva**, stretched between two fingers, develops a "beads-on-a-string" structure as it thins, like those shown in Fig. 1.6. This is characteristic of dilute polymer solutions, whose viscosity thins like shampoo under *shear* flows, but *thickens* under *extensional* flows. In extensional flows, polymers are stretched along the flow direction (Fig. 1.7), and thus act directly against the flow as they try to recoil. The stronger the flow, the further they deform, and the harder they fight the flow. This behavior is described by a rate-dependent extensional viscosity $\eta_E(\dot{e})$.

- Concentrated **cornstarch** solutions, known as oobleck to parents of young children, *shear thicken* dramatically: The apparent
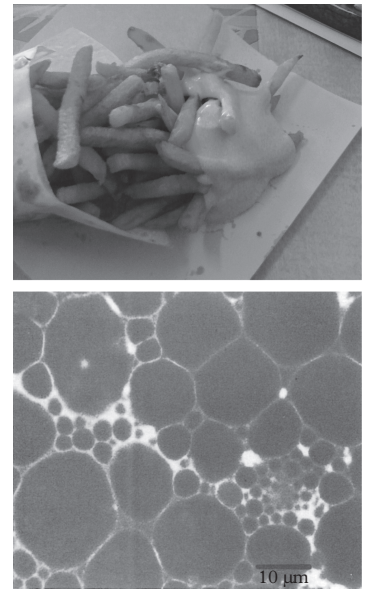

Fig. 1.4 *Mayonnaise cools your fries without flowing off. Its yield stress is a result of jammed oil droplets, shown in a confocal micrograph. The water phase contains a fluorescent dye, while the oil droplets are dark. Some may prefer ketchup, another yield stress material. Micrograph reprinted from Food Structure, 1, Heertje, I., Structure and function of food products: A review, pp. 3–23, Copyright (2014), with permission from Elsevier.*
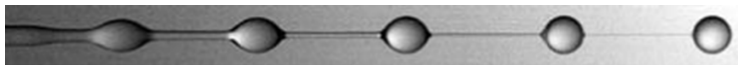
Fig. 1.6 *High-speed video images of "beads-on-a-string" forming on a jet of dilute polymer solution. From Clasen, C., Eggers, J., Fontelos, M. A., Li, J., & McKinley, G. H.* J. Fluid Mech, **556**, 283–308 2006a *reproduced with permission.*
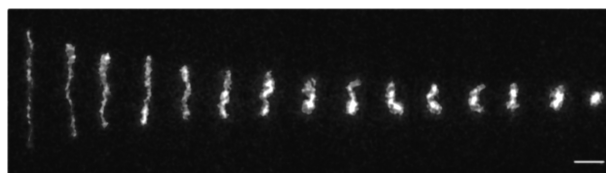
Fig. 1.7 *Flourescence microscopy images of a lambda phage DNA (48.5 kbp) molecule relaxing. The polymer chain is sub-jected to an extensional flow and high degrees of extension, followed by direct imaging of its relaxation into a coiled state after the cessation of flow. The scale bar is 5 μm. Image courtesy of Yuecheng (Peter) Zhou and Charles M. Schroeder.*

shear viscosity can jump a million-fold when the material is sheared above a critical rate. This reflects a competition between shear-driven cluster formation of aggregating particles (increas-ing the resistance to flow) and relaxation to equilibrium (re-ducing the resistance). As with shear thinning materials, shear thickening is described by a rate-dependent shear viscosity $\eta(\dot{\gamma})$.

- **Jello** is made by cooling an initially-heated gelatin solution. Although the solution cools relatively quickly (minutes), the material transitions from a viscous liquid to an elastic solid over a time scale of hours. A *gelation* process occurs gradually, as suspended polymers, a mix of denatured protein and peptide fragments, cross-link to form ever-larger clusters, eventually spanning the entire material. Rheological characteristics of interest include the *gel time* τ_G, and frequency-dependent viscoelastic moduli $G^*(\omega)$, especially its elastic modulus. After all, this is what gives jello its gentle jiggle—and the ability to suspend solid pieces of fruit.

- **Egg whites** are viscoelastic solutions of protein in water whose rheology enables some culinary feats (*e.g.*, merengues) while frustrating even simple tasks (*e.g.*, removing small bits of

egg shell, or climbing up mixers and making a mess). This rod-climbing "Weissenberg effect" occurs due to *normal stress differences*: Shearing the solution stretches its elastic elements in the flow direction. As they recoil, they tend to raise the material's tension in the flow direction (around the rod), relative to the gradient direction (along the rod), which squeezes egg white up the spinning rod. The rheological quantity responsible for this behavior is the normal stress difference $N_1 \dot{\gamma}^2$. Additionally, whip the egg white, and it forms a long-living foam. Proteins at the surface are exposed to air, denature, and aggregate to form an interfacial shell with its own **surface viscoelasticity,** which can be described by surface shear moduli $G_s^*(\omega)$.

These examples—and many more—provide some sense of the wide variety of phenomena encompassed within the rich world of rheology. Many of the materials listed elude the conventional classification of matter into "solid, liquid, or gas" phases. Instead, these soft materials usually consist of multiple components, each of which can be described individually as a liquid, solid, or perhaps as a macromolecule. These components form a mesoscopic structure within the material that is not immediately apparent to our senses of touch or sight, since they typically form on the nanometer to micrometer scale. These structures give rise to the rich set of dynamic response properties already described, that are not found in simple fluids or solids. "Macroscopic" experimental tools—*e.g.*, our fingers as they manipulate shampoo, or the rheometers described in Section 1.2.2—measure an "averaged" response of heterogeneous materials, which behave like homogeneous, continuum effective materials on those macroscopic length scales.

1.2.1   Linear and nonlinear rheology

The rheology of a material is measured by relating the stress, σ to the imposed deformation strain γ or rate of strain $\dot{\gamma} = d\gamma/dt$. A simple representation of the measurement is shown in Fig. 1.8, in which a force F_x is required to pull a plate of area A_y (the "y" denotes the direction of the outward unit normal vector). The plate, separated from a bottom plate by a distance δ_y, moves a distance Δx. The shear stress is

$$\sigma_{yx} = F_x/A_y \tag{1.6}$$

and the strain

$$\gamma = \Delta x/\delta_y. \tag{1.7}$$

| stress | $\sigma_{yx} = F_x/A_y$ |
| strain | $\gamma = \Delta x/\delta_y$ |
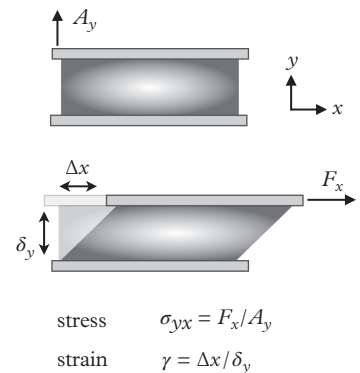
Fig. 1.8 *Shear deformation of a material between two parallel plates.*

If the material between the plates were an elastic solid, the strain would reach a steady value for a given stress. If the material were a viscous fluid, the strain would represent the deformation at a finite time, and the plate would continue to move to the right at a shear rate $\dot{\gamma} = \sigma/\eta$. Both behaviors are analogous to the movement of our probe particle in Fig. 1.1.

Linear response properties, most commonly the frequency-dependent linear viscoelastic moduli $G^*(\omega)$, reflect the response of materials to negligibly small departures from equilibrium (departures which, in fact, arise spontaneously due to the material's thermal energy). These properties reflect the relaxation processes that occur within such materials in their equilibrium state. With knowledge of the microstructural elements and their organization, important static and dynamic structural features can be determined from measurements of $G^*(\omega)$. For example, the Rouse or Zimm models can be used to determine the molecular weight and concentration of polymers in solution, or relaxation times for polymer entanglements. Hydrodynamic calculations for solid particles or liquid droplets with viscosity η and interfacial tension can be used to extract the size distributions of droplets or particles from $G^*(\omega)$ measurements made on particle suspensions or concentrated emulsions.

Additionally, linear-response properties like $G^*(\omega)$ can be used to measure other material properties of evolving materials (*e.g.*, materials like yoghurt or clay that age after being sheared, or like Jello that undergoes a sol-gel transition), so long as the evolution occurs on time scales longer than is required to actually make such measurements.

Nonlinear response properties arise when the microstructure of the material is driven significantly out of equilibrium. The yield stress σ_y requires the material to be strained far enough for microstructural elements to break or rearrange. Shear thinning and shear thickening viscosities and extension thickening arise when an imposed flow alters the arrangement of microstructural elements from their equilibrium distribution, making the flow easier or harder to maintain. Normal stress differences N_1 and N_2 arise when the equilibrium microstructure is deformed enough to drive anisotropic tension within the material.

Nonlinear-rheological quantities like yield stresses, rate-dependent viscosities, and normal stress coefficients cannot be determined using linear-response measurements. In a few cases and in certain limits, correspondences may exist between linear and nonlinear properties. For example, the low-$\dot{\gamma}$ limit of the first normal stress coefficient of a viscoelastic liquid is related to the low-frequency limit of the elastic modulus $G'(\omega)$, via

$$\lim_{\dot{\gamma} \to 0} \frac{N_1(\dot{\gamma})}{\dot{\gamma}^2} \Leftrightarrow \lim_{\omega \to 0} \lim \frac{G'(\omega)}{\omega^2}. \qquad (1.8)$$

The Cox–Merz rule is an empirical relation relating the frequency-dependent complex viscosity

$$\eta^*(\omega) = \frac{G^*(\omega)}{i\omega} \qquad (1.9)$$

to the rate-dependent steady-shear viscosity $\eta(\dot{\gamma})$, according to

$$\eta(\dot{\gamma}) = \left| \eta^*(\dot{\gamma}) \right| \quad \text{(Cox-Merz)}, \qquad (1.10)$$

but does not always apply.

More generally, however, there is no way to determine nonlinear response properties from linear response measurements. On a qualitative level, toothpaste appears to behave like Jello according to linear viscoelastic measurements. Both are soft, viscoelastic solids under weak forcing. Unlike jello, given enough force, toothpaste flows—it has a yield stress—while jello will fracture and break.

1.2.2   Linear response measurements

Linear response measurements perturb a material so slightly that its equilibrium structure remains almost entirely unchanged, driving small deformations that subsequently relax. Even when a soft material is unforced, and simply sitting in equilibrium at some temperature T, it constantly experiences weak, stochastic-thermal forces that drive small-amplitude deformations of the sort used to measure linear response properties. Passive microrheology exploits these thermal fluctuations as a built-in source of small-amplitude forces to reveal (and measure) the linear viscoelastic response properties of the material.

A mechanical rotational rheometer provides a means of generating shear strains and measuring stress by the torque imposed on the tool. Mechanical rheometers employ a variety of tool geometries—*e.g.*, cone-and-plate, cylindrical, and parallel plate. These geometries are shown in Fig. 1.9. Each has its particular operating regimes of frequency, shear amplitude, shear rate, and sample properties—an operating regime—but all those shown here are designed to excite purely shear strains. The flow kinematics are determined solely by the geometry.

concentric cylinder

double wall

cone-and-plate

parallel plate
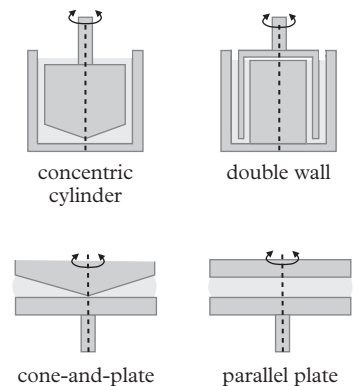
Fig. 1.9 *Common tool geometries of rotational mechanical rheometry.*

Complex shear modulus

A typical rheometry measurement imposes an oscillatory strain

$$\gamma(t) = \gamma_0 e^{i\omega t}, \tag{1.11}$$

with amplitude γ_0 and frequency ω, and measures the stress $\sigma(t)$ in response. In any linear response measurement, the measured stress will oscillate sinusoidally with the same frequency ω (with no harmonics),

$$\sigma(t) = \sigma_0 e^{i(\omega t + \delta)} \tag{1.12}$$

with an amplitude σ_0 and phase lag (or loss tangent) δ that encodes the rheology of the material itself. A purely elastic material is one for which $\delta = 0$: The stress is directly proportional to the strain. A purely viscous material is one for which $\delta = \pi/2$: The stress is proportional to the *rate of strain*. At the height of the strain oscillation, the shear rate is zero, and thus the stress. By contrast, the strain rate (and thus the viscous stress) is largest at zero strain.

Measuring stress as a function of strain over a range of frequencies ω gives the linear, viscoelastic moduli, encompassed in the complex shear modulus $G^*(\omega)$, defined by

$$G^*(\omega) = \frac{\sigma(t)}{\gamma(t)} = \frac{\sigma_0 e^{i\delta}}{\gamma_0}. \tag{1.13}$$

The complex shear modulus $G^*(\omega)$ is the frequency-dependent equivalent of a pure elastic modulus, defined as the shear stress divided by the shear strain. The higher G^*, the more stress is required to drive a certain strain.

We could just as easily take the same measured data, but instead compare the measured stress $\sigma(t)$ with the *strain rate*,

$$\dot{\gamma}(t) = i\omega\gamma_0 e^{i\omega t} \equiv i\omega\gamma(t) \tag{1.14}$$

as would make sense for a viscous or viscoelastic liquid. The complex viscosity is then obtained by dividing the stress by the strain rate,

$$\eta^*(\omega) = \frac{\sigma_0 e^{i\delta}}{i\omega\gamma_0}. \tag{1.15}$$

Comparison with eqn 1.13 reveals the complex shear modulus and complex viscosity to be trivially related:

$$G^*(\omega) = i\omega\eta^*(\omega). \tag{1.16}$$

This is significant, because it underscores the fact that $\eta^*(\omega)$ contains exactly the same information as $G^*(\omega)$. This should not be surprising—after all, precisely the same measurement gave rise to both quantities.

The complex modulus is often split into real and imaginary components

$$G^*(\omega) = G'(\omega) + iG''(\omega), \qquad (1.17)$$

which separates out the elastic (or storage) modulus $G'(\omega)$ and the viscous (or loss) modulus $G''(\omega)$. The storage modulus $G'(\omega)$ is precisely the conventional elastic shear modulus, generalized to allow for frequency dependence, and describes the (recoverable) energy required to deform the material at a particular frequency. $G'(\omega)$ represents the portion of the shear stress that varies in-phase with the sinusoidal shear strain. By contrast, the loss modulus $G''(\omega)$ describes the (irrecoverably lost) energy that is dissipated as a material deforms at a given frequency. It is 90 degrees out-of-phase with the shear strain, or equivalently, in-phase with the shear rate. The loss modulus is intimately related to the real part of the frequency-dependent complex viscosity,

$$G''(\omega) = \omega\eta'(\omega), \qquad (1.18)$$

as can be seen from eqn (1.16). Here, we have split η^* into its real and complex parts, via

$$\eta^*(\omega) = \eta'(\omega) + i\eta''(\omega), \qquad (1.19)$$

by analogy with (1.17). The phase lag or phase angle δ in (1.12) is related to the storage and loss modulus via

$$\tan\delta(\omega) = \frac{G''(\omega)}{G'(\omega)}, \qquad (1.20)$$

ranging from $\delta = 0$ for purely elastic materials, whose stress varies in-phase with strain, and $\delta = \pi/2$ for viscous fluids, whose stress is 90 degrees out-of-phase with the applied strain (which means, of course, that $\tan\delta$ diverges as $G' \to 0$).

More generally, any time-dependent stress $\sigma(t)$ can be decomposed into frequency-dependent components through a Fourier Transform:

$$\sigma(t) = \frac{1}{2\pi}\int_{-\infty}^{\infty} \tilde{\sigma}(\omega)e^{i\omega t}d\omega. \qquad (1.21)$$

So long as the total strain is small enough for the linear response approximation to remain valid, the stress driven by each of these strain

oscillations is given by eqn 1.13, and the total stress at any given time is given by the superposition of each oscillating component,

$$\sigma(t) = \frac{1}{2\pi} \int_{-\infty}^{\infty} G^*(\omega)\tilde{\gamma}(\omega)e^{i\omega t}\,d\omega. \tag{1.22}$$

Using the convolution theorem, eqn 1.22 can be re-expressed as

$$\sigma(t) = \int_{-\infty}^{\infty} m(t-t')\gamma(t')\,dt', \tag{1.23}$$

where the memory function

$$m(t) = \frac{1}{2\pi} \int_{-\infty}^{\infty} G^*(\omega)e^{i\omega t}\,d\omega \tag{1.24}$$

is the inverse Fourier Transform of the complex modulus $G^*(\omega)$. Physically, $m(t-t')$ expresses how much the stress at any given time t "remembers" a deformation that happened at some previous time t'. Because the stress can't "remember" a deformation that has not yet occurred, $m(t-t')$ must be zero for all $t' > t$, a property of *causal* functions. Equation 1.23 is thus often written as

$$\sigma(t) = \int_{-\infty}^{t} m(t-t')\gamma(t')\,dt'. \tag{1.25}$$

Alternatively, stress may be related to the previous *shear rate* history,

$$\sigma(t) = \int_{-\infty}^{\infty} G(t-t')\dot{\gamma}(t')\,dt', \tag{1.26}$$

where $G(t-t')$ is called the *relaxation modulus*, and expresses how well the stress at time t "remembers" the shear rate at a previous time t'. Using the convolution theorem, eqn 1.26 becomes

$$\sigma(t) = \int_{-\infty}^{\infty} \mathscr{F}\{G(t)\}i\omega\tilde{\gamma}(\omega)e^{i\omega t}\,d\omega. \tag{1.27}$$

Comparison with eqn 1.22 reveals the Fourier Transform of $G(t)$ to be

$$\mathscr{F}\{G(t)\} = \frac{G^*(\omega)}{i\omega} = \eta^*(\omega), \tag{1.28}$$

by definition of the complex viscosity $\eta^*(\omega)$, eqn 1.16.

This set of definitions can seem arbitrary or confusing at first. In short, two Fourier Transform pairs exist:

$$m(t) = \mathscr{F}^{-1}\{G^*(\omega)\} \tag{1.29}$$

$$G(t) = \mathscr{F}^{-1}\{\eta^*(\omega)\}. \tag{1.30}$$

One Fourier Transform pair, $G^*(\omega)$ and $m(t)$, is best suited for viscoelastic solids, but is used almost ubiquitously in rheology. The other Fourier Transform pair, $\eta^*(\omega)$ and $G(t)$, is better suited for viscoelastic liquids. Unfortunately, this convention can be quite confusing, since one might naturally expect $G^*(\omega)$ to represent the Fourier Transform of $G(t)$, from a purely notational standpoint. This is not true, so take note.

Kramers–Kronig relations

The storage and loss moduli are not independent functions, since the dynamic response they encode is *causal*—a material can not respond to a stimulus that has not yet occurred. Consequently, the memory function $m(t)$ *must* be zero for all $t < 0$. From complex analysis, this implies that $G^*(\omega)$ is analytic in the lower-half plane. Moreover, the real and imaginary parts of $G^*(\omega)$—namely, $G'(\omega)$ and $G''(\omega)$—are related exactly by the Kramers–Kronig relations (McQuarrie, 2000; Landau *et al.*, 1986)

$$G'(\omega_0) = -\frac{1}{\pi}\mathscr{P}\int_{-\infty}^{\infty}\frac{G''(\omega)}{\omega - \omega_0}d\omega \tag{1.31}$$

$$G''(\omega_0) = \frac{1}{\pi}\mathscr{P}\int_{-\infty}^{\infty}\frac{G'(\omega)}{\omega - \omega_0}d\omega, \tag{1.32}$$

where the $\mathscr{P}$ denotes the Cauchy Principle Value of the integral.[5] These are derived in Appendix A.3. Booij and Thoone (1982) derived various alternative forms of the Kramers–Kronig relations that are of particular benefit to rheologists, including

$$G''(\omega) = \frac{2\omega}{\pi}\int_{0}^{\infty}\frac{G'(u) - G'(\omega)}{u^2 - \omega^2}du \tag{1.33}$$

$$G'(\omega) = G'(0) - \frac{2\omega^2}{\pi}\mathscr{P}\int_{0}^{\infty}\frac{G''(u)/u - G''(\omega)/\omega}{u^2 - \omega^2}du \tag{1.34}$$

$$G'(\omega) = G'(\infty) - \frac{2}{\pi}\mathscr{P}\int_{0}^{\infty}\frac{uG''(u) - \omega G''(\omega)}{u^2 - \omega^2}du. \tag{1.35}$$

[5] The Cauchy principal value integral accounts for the singularity at $\omega' = \omega$,

$$\mathscr{P}\int_{0}^{\infty}f(\omega')d\omega'$$
$$= \lim_{\varepsilon \to 0^+}\left[\int_{0}^{\omega-\varepsilon}f(\omega')d\omega' + \int_{\omega+\varepsilon}^{\infty}f(\omega')d\omega'\right].$$

The Kramers–Kronig relations provide an important validation of measurements or calculations of the viscoelastic moduli and are the basis for calculating the moduli in techniques such as laser tracking microrheology, which is discussed in Chapter 6.

As we have seen, the memory function $m(t)$ contains precisely the same information as $G^*(\omega)$, which should be obvious given that they form a Fourier Transform pair. The complex viscosity $\eta^*(\omega)$ and relaxation modulus $G(t)$ likewise contain the same information. Since $G(t) = dm/dt$, however, $m(t)$ can only be determined from $G(t)$ up to an additive constant, as seen directly in eqns 1.34 and 1.35. Either the zero-frequency $G'(0)$ or infinite-frequency $G'(\infty)$ must be supplied to fully determine the elastic modulus $G'(\omega)$ from the loss modulus $G''(\omega)$.

Creep Compliance

By now it should be clear that there are a great many equivalent representations of a material's linear-viscoelastic response, each of which contains the same fundamental information, yet some arise more naturally in particular contexts, and are therefore more natural to interpret or manipulate than others.

The creep compliance $\mathcal{J}(t)$ is one functional representation of a material's linear viscoelastic properties that will be particularly useful for passive microrheology. The creep compliance $\mathcal{J}(t)$ is the strain that results following a suddenly-imposed stress of unit magnitude,

$$\sigma(t) = H(t), \tag{1.36}$$

where $H(t)$ is the Heaviside step function, then measuring the strain response

$$H(t) = \int_{-\infty}^{t} m(t - t')\mathcal{J}(t')dt'. \tag{1.37}$$

Fourier Transforming gives

$$\frac{1}{i\omega} = G^*(\omega)\tilde{\mathcal{J}}(\omega), \tag{1.38}$$

revealing the transformed creep compliance to be related to the complex modulus via

$$\tilde{\mathcal{J}}(\omega) = \frac{1}{i\omega G^*(\omega)}, \tag{1.39}$$

or equivalently

$$\mathcal{J}(t) = \mathcal{F}^{-1}\left(\frac{1}{i\omega G^*(\omega)}\right).$$

(1.40)

This relation will facilitate the interpretation of microrheology measurements. In particular, the mean squared displacement $\langle\Delta r^2(t)\rangle$ of a tracer particle in an equilibrium material turns out to be directly proportional to the creep compliance $\mathcal{J}(t)$.

Two limiting cases are revealing. A Newtonian fluid with viscosity η, and complex modulus $G^* = i\omega\eta$, has creep compliance

$$\mathcal{J}(t) = \frac{t}{\eta} \quad \text{(Newtonian fluid)}$$

(1.41)

that grows linearly (and unbounded) in time. An elastic solid with shear modulus G has a creep compliance

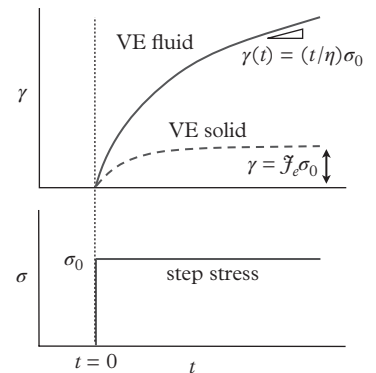$$\mathcal{J}(t) = \mathcal{J}_e = \frac{1}{G} \quad \text{(Elastic solid)}$$

(1.42)

that is constant in time. Examples for viscoelastic liquids and solids are shown in Fig. 1.10: At long times, each $\mathcal{J}(t)$ asymptotes to the appropriate limit of a viscous fluid or an elastic solid.

1.2.3 Nonlinear-rheology measurements

Shear thinning and thickening

Nonlinear measurements are fundamentally different and require different techniques, since the material is typically driven far out of equilibrium. Here we will review a few examples of nonlinear-rheological behavior to give the reader a sampling of the phenomena that are of interest and issues that arise in their measurement. A large body of work in the rheology literature deals with nonlinear phenomena that arise in polymer processing, but materials like polymer melts are generally far outside the operating regime of microrheology. We will consider a few examples of materials that have been investigated in microrheology experiments and are discussed later in the book: The shear thinning of suspensions and measurements of yield stresses.

Shear-dependent viscosities are measured using a continuous deformation at different shear rates $\dot{\gamma}$. In a material that exhibits **shear thinning**, the viscosity decreases with increasing shear rate. Figure 1.11 shows viscosity measurements from the classic study of Choi and Krieger (1986*b*), who measured the shear thinning of polymer-stabilized PMMA nanoparticles suspended in silicone oil.

Fig. 1.10 *The material strain* $\gamma(t)$ *from an applied step stress* σ_0 *for a viscoelastic liquid and viscoelastic solid.*

Fig. 1.11 *The relative viscosity $\eta_r = \eta/\eta_s$ of colloidal suspensions exhibits* shear thinning *as the shear stress increases. Reprinted from* J. Colloid Interface Sci., *113, Choi, G. N. & Krieger, I. M., Rheological studies on sterically stabilized dispersions of uniform colloidal spheres. II. Steady-Shear Viscosity, pp. 101–13, Copyright (1986), with permission from Elsevier.*
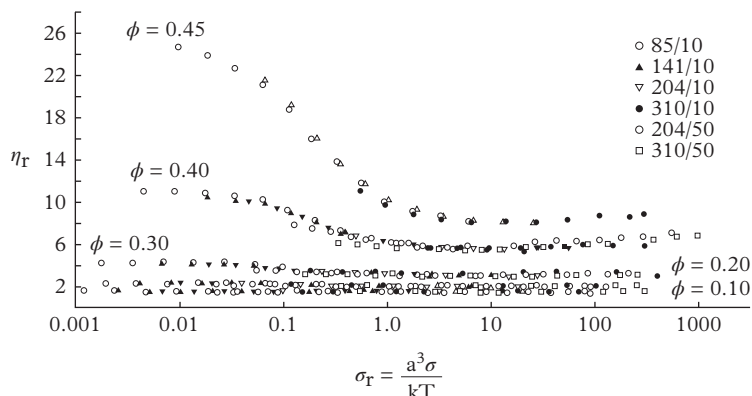
In suspensions, shear thinning occurs due to the reorganization of particles along the shear gradient. Two limits are observed: At low shear rates, the material has a viscosity η_0 that reflects the equilibrium structure of the suspension. At high shear rates, the nonequilibrium structure is fully formed, and the high-shear viscosity is η_∞. The empirical Cross model can faithfully describe data such as that shown in Fig. 1.11,

$$\frac{\eta - \eta_\infty}{\eta_0 - \eta_\infty} = \frac{1}{1 + K\dot{\gamma}^{1-n}} \tag{1.43}$$

but detailed microscopic models that accurately account for the Brownian and hydrodynamic origins of the high- and low-shear viscosities have also been developed (Brady, 1993).

At still higher shear rates, suspensions sometimes exhibit **shear thickening**, in which the viscosity again increases. Modest shear thickening is expected to occur due to lubrication hydrodynamic forces between particles, which causes them to form "hydroclusters" that disrupt the high-shear nonequilibrium microstructure (Egres and Wagner, 2005; Wagner and Brady, 2009). At high concentrations, suspensions shear thicken strongly, or "discontinuously" (D'Haene *et al.*, 1993).

Yield stress

A material with a yield stress behaves as a soft solid under weak stress, but flows like a fluid at high-enough stress (Møller *et al.*, 2006; Denn and Bonn, 2011). Foods like mayonnaise and ketchup have yield stresses, as do foams, toothpaste, and many paints (the paint flows from the brush onto the wall, but not down to the floor!) Yield stresses are frequently engineered into materials to suspend particles, like

droplets of silicon oil in conditioning shampoos, solid rock cuttings in drilling muds, or crystallites of active crop protectant for agricultural treatments. Common yield stress fluids include suspensions of associative hydrocolloids such as xanthan and other biopolymer "gums," cellulose fibers, swellable microgel particles (like Carbopol), associative colloids, and natural or synthetic clays—bentonite, kaolin, and the synthetic clay Laponite.

To model a fluid with a yield stress σ_y, several variants on the general constitutive relation,

$$
\begin{aligned}
\dot{\gamma} &= 0 & \sigma &\leq \sigma_y \\
\sigma &= \sigma_y + f(\dot{\gamma}) & \sigma &> \sigma_y.
\end{aligned}
\tag{1.44}
$$

are commonly used. If the flowing state behaves as approximately Newtonian, then this gives the Bingham fluid,

$$
f(\dot{\gamma}) = \eta_p \dot{\gamma}.
\tag{1.45}
$$

Yield stress fluids that behave as power-law fluids when flowing are described by the Herschel–Bulkley model,

$$
f(\dot{\gamma}) = k \dot{\gamma}^n.
\tag{1.46}
$$

Both models satisfy the conditions that $f(0) = 0$, which defines a consistent yield stress, and $df/d\dot{\gamma} > 0$, which is required for mechanical stability.

Yield stress fluids present several vexing problems in bulk rheometry, as discussed by Møller *et al.* (2006), which may be expected to complicate microrheology experiments as well. Wall slip is a common artifact, and frequently accomodated by using roughened tools or vane geometries, although the latter do not provide a direct measurement of the shear strain (Dzuy and Boger, 1983; Nguyen and Boger, 1992; Barnes and Nguyen, 2001). Additionally, shear banding or even fracture may occur within the material.

Different strategies have been employed to measure yield stresses. One set of techniques starts with a stationary material, then gradually increasing the applied stress until the material flows. Alternatively, the strain or strain rate may be imposed, *e.g.*, starting from a steadily flowing system, and gradually reducing the strain rate. Typically, the resulting stress approaches a constant value (Fig. 1.12) as the strain rate approaches zero. Such measurements suggest an apparent viscosity that diverges with decreasing (Moller *et al.*, 2009). Corresponding linear, frequency-sweep measurements of $G^*(\omega)$ show the material does indeed behave as a soft solid.
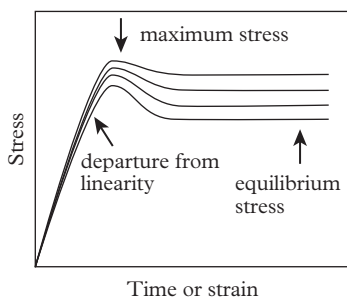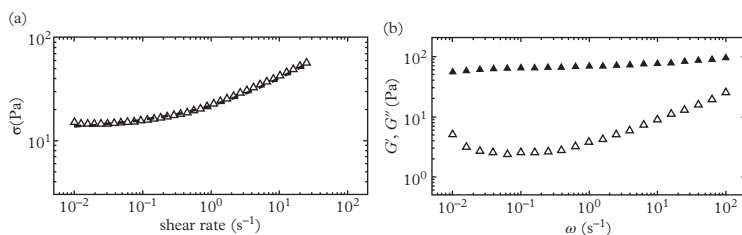
Fig. 1.13 *Different definitions of the yield stress.*

The yield stress measurements described typically report different yield stress values, depending on whether measurements start from flowing or quiescent states (Fig. 1.13). In some cases, the yield stress is defined as the value where the stress departs from linearity, or as the maximum measured stress (if a maximum occurs). Those two quantities are called the *static* yield stress, since they are measured starting from a quiescent state. They stand in contrast to the *dynamic* yield stress, which are measured by starting with a flowing state, decreasing the shear rate to $\dot{\gamma} = 0\,s^{-1}$, and extrapolating the measured stress.

Thixotropy

Closely related to yield stress is **thixotropy**, which refers to a history-dependence in the measured rheology. In fact, thixotropy and yield stresses are often (but not always) found together. Thixotropy arises due to reversible (and irreversible) microstructural changes in the material that grow an ever-stiffening mesostructural network over time. The yield stress of such materials increases gradually (often logarithmically in time) as they are left to rest. When forced to flow, these networks are broken to an extent that depends upon their strength, the strength of the flow, and time scales for aging (network rearrangement or build-up) to occur.

Experimentally, thixotropic behavior is detected by imposing an increasing set of shear stresses on the material, and measuring the resulting shear rate, then reversing the stress ramp to return back to the non-flowing state. Thixotropic materials produce a strong hysteresis during this cycle, whereas non-thixotropic materials do not (Fig. 1.14). One can thus draw a distinction between simple, or "ideal" yield stress materials like foams, emulsions, and microgel suspensions like Carbopol, which exhibit little or no hysteresis during this stress ramp cycle, and thixotropic yield stress materials like colloidal or fibrous gels, associative polymers, and clays (such as bentonite), which are strongly thixotropic (Moller *et al.*, 2009).

Extensional rheology

Unfortunately, a material's nonlinear-shear rheology cannot be used to predict its nonlinear extensional rheology. In fact, materials with appreciable elasticity may *extension thicken* significantly under extensional flows, despite having viscosities that *shear thin* just as dramatically. Strong extension thickening makes a material very difficult to pump through porous media or filters, and causes "beads-on-string" morphologies in viscoelastic fluid threads (Fig. 1.6), whereas Newtonian fluid threads would break into drops (Clasen *et al.*, 2006*a*).

Different techniques are required to probe the extensional rheology of materials, since the material must be subjected to a controlled extensional flow (Fig. 1.15). During this flow, the strain on the material grows exponentially in time in one direction, while contracting exponentially in the other direction(s). Extensional rheometry is far more challenging than shear rheometry in this regard: While a shear rheometer can impose arbitrarily large strain by simply rotating a cone or concentric cylinder indefinitely, geometric and practical constraints limit the spatial extent over which extensional rheometers can stretch a material with exponentially-growing strain. Strategies employed to do so include filament stretching rheometry (FISER) and capillary breakup extensional rheometry (CABER), which impose controlled extensional strains (McKinley and Sridhar, 2002; Bhardwaj *et al.*, 2007). Microfluidic methods have also been introduced (Pipe and McKinley, 2009). Our point is not to delve into a detailed discussion of extensional rheometry, but instead to highlight the difficulties associated with precise measurements of even the second paradigmatic type of flow for complex fluids. As with nonlinear shear rheometry measurements, nonlinear extensional rheology measurements require a system that has been carefully designed to excite only a particular flow type, to measure the response, and to interpret the results in terms of an intrinsic material property.

1.3 Colloidal particles

Microrheology, whether passive or active, is based on measurements of the motion of colloidal probe or tracer particles ranging in size from roughly 0.1–10 μm (Fig. 1.16). In Chapter 2, we discuss the mechanics of probe motion that underlie all microrheological methods. In this section, we will briefly review the chemical and physical properties of probe particles.
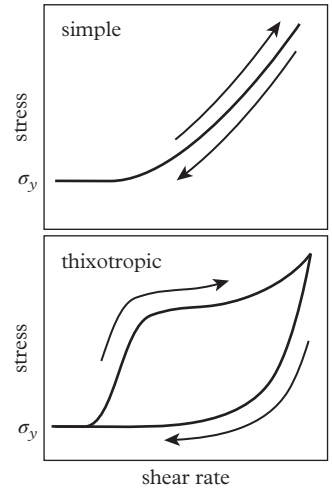

Fig. 1.14 *Stress ramp experiments, in which applied shear stress increases in steps from zero to a maximum value, then is decreased through the same series, reveal no hysteresis in simple yield stress materials, but strong hysteresis in thixotropic materials like suspensions of clay particles. Both materials have a finite yield stress σ_y.*
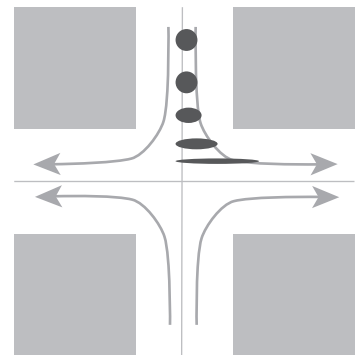
Fig. 1.15 *Purely extensional deformations, like those near the center of a cross-slot geometry of two converging flows, probe extensional rheology. A material element is shown deforming in the extensional flow.*

UDEL   LEI   2.0kV   ×10,000 WD 7.9mm   1μm

Fig. 1.16 *Scanning electron micrograph of uniform polystyrene latex particles with diameter 1.6 μm.*
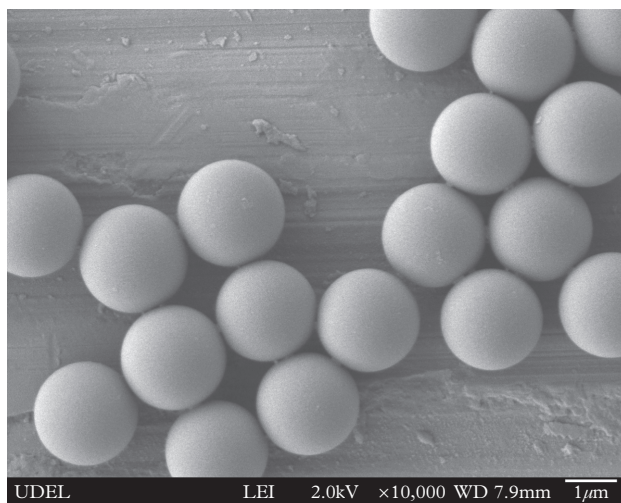
Colloid refers to the Greek word for glue, κολλα, and is attributed to the Scottish chemist Thomas Graham (1805–69).[6] In his studies of dialysis, Graham observed that some of his solutions were unable to pass through a parchment membrane (Graham, 1861; Graham, 1864). These solutions, which he recognized as suspensions of microscopic particles, stayed put on one side of the membrane, bound as if held together or "glued." During the same period, Robert Brown (1773–1858) strengthened the connection between colloids and a characteristic length scale of matter (Brown, 1828). Brown did not adopt Graham's term, but instead referred to these small, seemingly animated particles as *molecules* during his own careful microscopy observations of their random motion. His work is why we now call the random thermal agitation of colloids *Brownian motion*, as seen in Figure 1.15.

A meticulous experimentalist, Brown, concluded that the random motion he observed was due to the small size of the particles. Brown ruled out that the composition or origin of the particles gave rise to their animation. It was not a characteristic of organic matter only—an important idea at the time, since others who had made similar observations had speculated that the spontaneous motion of organic particles was a manifestation of the "vital force" that distinguished animated matter (living things) from inanimate matter.[7] Brown carefully ground all sorts of materials into fine particles, some derived from organic matter and transformed organic matter (such as coal), and others from minerals, rocks, and even a small piece of the great Sphinx of Giza. He concluded that particles on the order of 1/30,000[th] to

[6] Graham served as a professor in Glasgow, then later at University College, London. In 1855 he became Master of the Mint, a position that Isaac Newton held.

[7] To place Brown's work in perspective, it came not long after the 1818 publication of Mary Shelley's *Frankenstein*, in which the protagonist is a scientist who develops a technique to impart life to non-living matter.

$1/20,000^{\text{th}}$ of an inch (0.85–1.3 μm), which he meticulously measured using a micrometer, will exhibit random motion in solution regardless of their origin. It was not until the work of Einstein, Sutherland, Langevin, Smoluchowski, and their contemporaries that the Brownian motion of colloids would be definitively explained by the thermal motion of the surrounding fluid molecules through the kinetic theory of heat. We return to this history when we discuss passive microrheology in Chapters 3–5.

Today we recognize colloids as a special division of matter—a length scale that exhibits molecular-scale processes like Brownian motion, but are many times larger than atomic or molecular dimensions. Accordingly, the IUPAC definition of colloidal is a "state of subdivision such that the molecules or polymolecular particles dispersed in a medium have at least one dimension between approximately 1 nm and 1 μm, or that in a system discontinuities are found at distances of that order" (Slomkowski *et al.*, 2011).

1.3.1   Colloidal probe chemistries

Colloidal particles are defined by their length scale, yet the applicable dimensions span a wide range, from nanometers to several micrometers, and can encompass different shapes, chemistries (inorganic, organic), and even phases (from fluid emulsion droplets to solid polymer particles). Here we will review the key attributes of colloidal probe particles used in microrheology experiments.

Colloids must exhibit three principal characteristics to be suitable for use as microrheological probes. First, the particles should be uniform in size and shape. Second, the probes should be stable against aggregation or chemical degradation, and must disperse well into the medium of interest. Third, the probe surface chemistry should not alter the local microenvironment. The first two issues are addressed here; the effect of surface chemistry on the probe microenvironment will be discussed further in Section 3.10.

The choice of particle chemistry depends on the material to be probed. Since many materials of interest to microrheology are aqueous, polymer latex microspheres, especially polystyrene, are a good and common choice. They are available from many commercial vendors and straightforward to synthesize. In general, polystyrene is stable, and its density ($\sim$1.05 g/cm^3) is close to that of room temperature water, which reduces (but does not eliminate) gravitational sedimentation of the probes.

In organic solvents, inorganic particles such as silica grafted with an organophilic layer or more solvent resistant resins like melamine and polymer latex such as poly(methylmethacrylate) (PMMA), are

a better choice. However, the density difference between inorganic particles and many organic solvents can lead to rapid probe sedimentation.

The microrheologist should assume that particles received as delivered from a manufacturer will contain impurities. These impurities will normally be surfactant stabilizers that keep particles dispersed during manufacture and storage. Surfactants and other residual impurities should be removed by a repeated centrifugation, decantation, and redispersion steps. The particles should be redispersed by gentle agitation into a solution, such as buffer, that closely matches the solution conditions of the final sample (washing methods are discussed further in Section 1.3.4). Care must be taken that the particles do not aggregate, especially if the ionic strength of the solution is high or the pH towards the extreme end. Most suspensions are stabilized, at least in part, by charges on their surface.

In Table 1.1, we summarize several physical properties of probe colloids that will be described in more detail.

Polystyrene

The synthesis of highly-uniform polystyrene latex is well established and many commercial vendors supply a variety of sizes as well as particles with modified surface chemistries. The particles are easily labeled with fluorescent dyes for particle tracking using fluorescence microscopes, and unlabeled particles readily scatter light due to the high contrast between indices of refraction ($n = 1.58$ for polystyrene, 1.33 for water). Finally, the surface chemistry of polystyrene particles can be controlled, by the adsorption of polymers and proteins, the addition of co-monomers during their synthesis, or through the reaction of chemically active sites on the particle surface. Commercial vendors supply particles ready for use as aqueous solutions at concentrations between 2.5–10 wt%. Because of the importance of polystyrene colloids, we will summarize their synthesis and chemical properties.

Table 1.1 *Common probe-particle chemistries and their physical properties.*

chemistry	density (g/cm³)	refractive index
polystryene (PS)	1.05	1.58
polymethylmethacrylate (PMMA)	1.19	1.49
melamine	1.57	1.68
silica	2.2	1.46
titania (anatase)	3.78	2.49

Polystyryene latex is synthesized by emulsion polymerization (Piirma and Gardon, 1976; Poehlein *et al.*, 1985; Candau and Ottewill, 1990). The monomer is dispersed as an emulsion, stabilized with surfactant, in a non-solvent (typically water). Adding an initiator (water soluble, in this case) generates an initial surge of free radicals, which begins to polymerize the monomer that has partitioned into the swollen micelles. As the polymerization reaction continues, adsorbed surfactant provides stability to the growing particles and bulk monomer emulsion providing a reservoir for growth until the monomer is depleted. The rapid particle-nucleation stage followed by a longer growth phase ensures a narrow range of particle diameters. It is also common to synthesize polystyrene latex using a surfactant-free polymerization process (Goodwin *et al.*, 1973).

Surface chemistry—The polymer chains in the particle begin and end with a functional group derived from the initiator, and, thus, the initiator used in the reaction imparts properties to the final particle, such as charged groups. The use of a sodium or potassium persulfate initiator, for instance, results in a significant coverage of negatively charged surface groups in the form of sulfonates, which are weak bases (conjugates to sulfonic acids, they are largely deprotonated, with pK_a values in the range of ~ 2). The typical charge densities on the particles are $\sigma = -1$ to -5 $\mu C/cm^2$, which confers good colloidal stability in water at low ionic strengths, as we will discuss in Section 1.3.3.

Other surface chemistries can be incorporated on polystyrene particles by using co-monomers with different functional groups (Table 1.2). Carboxylate (COOH) surface chemistries are introduced by the inclusion of acrylic acid monomer (typically $< 5\%$) in the particle synthesis (Poehlein *et al.*, 1985). Care must be taken when describing the surface chemistry of such particles, since it can be composed of the monomer-derived groups in addition to surface groups from the initiator, like sulfonates. This fact is often ignored in the microrheology literature, as surface chemistries are rarely as pure as envisioned. Water soluble polymer and monomer left over from the polymerization reaction may also be present on the particles, which requires careful cleaning before they are used. Another common chemistry is polystyrene with primary amine surface groups (Cousin and Smith, 1994; Voorn *et al.*, 2005). These are used either as positively charged particles or for amine reaction coupling chemistries. Because latex spheres are used in a number of biotechnology applications, such as immunodiagnostic assays and agglutination tests (Pichot, 2004; Tadros, 1993), particles are available with a number of other reactive surface chemistries, including epoxy, chloromethyl, chlorosulfonyl, aldehyde, and mercapto groups.

Table 1.2 *Polystyrene latex surface chemistries used in microrheology. Some arise during the chemical synthesis itself, whereas others are attained through modification steps, including adsorption or grafting.*

sulfonate	$(-SO_3^-)$
carboxylate	$(-COOH)$
amine	$(-NH_2)$
PEG	
BSA	
poly-lysine	

Adsorption—The hydrophobic nature of polystyrene latex enables a number of surface modifications by physical adsorption in aqueous media, most prominently by the adsorption of polyelectrolytes and proteins (Fig. 1.17). For microrheological studies of F-actin, McGrath *et al.* (2000) adsorbed poly-L-lysine, a cationic polymer, onto polystyrene probes. The adsorbed polyelectrolyte reverses the particle charge (Blaakmeer *et al.*, 1990) and increases the interactions between probes and the negatively charged proteins of the entangled network. Conversely, the protein bovine serum albumin (BSA) has been pre-adsorbed to probes to reduce their interaction with F-actin filaments by blocking the surface (McGrath *et al.*, 2000; Valentine *et al.*, 2004; Chae and Furst, 2005).

Adsorbed or grafted polymer layers can also be used to improve the stability of colloids at high ionic strengths or in organic solvents (Napper, 1983).

Covalent coupling—Covalent coupling reactions are another method for modifying probe surface chemistry (Ikada, 1994). One common chemistry is the covalent coupling reaction of poly(ethylene glycol) (PEG) to surface chemical moieties (McGrath *et al.*, 2000; Valentine *et al.*, 2004). Typically, PEG molecules, usually with molecular weights in the range of several thousand daltons, are grafted by N-hydroxysuccinimide ester-amine reactions using PEG-succinimidyl carboxyl methyl ester. The resulting PEG-decorated probes exhibit lower protein adsorption and have been used in microrheology studies of protein filaments and filamentous viruses (Valentine *et al.*, 2004; He and Tang, 2011; Sarmiento-Gomez *et al.*, 2012). Others have attached PEG by physically trapping an adsorbed triblock co-polymer, poly(ethylene glycol)-*b*-poly(propylene glycol)-*b*-poly(ethylene glycol), by swelling the particles with toluene, which allows the hydrophobic blocks to migrate into the probes, then removing the swelling solvent (Kim *et al.*, 2005; Sato and Breedveld, 2006). These particles remain stable even at high-ionic strength, which, as we will see in Section 1.3.3, indicates that the grafted polymer provides sufficient steric forces between the particles in addition to reducing the adsorption of species like proteins.
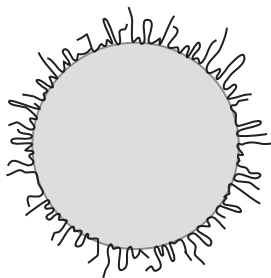
Fig. 1.17 *Adsorbed polymers and proteins or chemically grafted polymers can be used to tailor the probe surface chemistry. The polymer chains are not shown to scale, but typically extend only nanometers from the surface.*

Silica

Like polystyrene polymer latices, inorganic silica particles are also commercially available in the micrometer-diameter size range as highly uniform suspensions in water. Silica can be rendered organophilic, and is of course impervious to swelling and dissolution in organic solvents. The chief drawback of silica and other metal oxide particles (like titania or zinc oxide) for microrheology is their

high density relative to water and many organic compounds, $\rho \approx 2.2$ g/cm^3, which leads to relatively rapid sedimentation in fluid samples.

Using the Stöber method, monodisperse silica is synthesized by a combined hydrolysis and condensation of a silicon alkoxide precursor in a mixture of water, ethanol, and ammonia (Stöber *et al.*, 1968; Van Helden *et al.*, 1981; Bogush *et al.*, 1988; Bogush and Zukoski, 1991). The hydrolysis of tetraethylorthosilica (TEOS) forms silanols while the condensation polymerization reaction produces siloxane bridges. In the reaction, ethanol serves a co-solvent for the mixture of alkoxide and water, which are otherwise immiscible. Ammonia acts as a catalyst to initiate the rapid nucleation of particles.

Silica particle surfaces are rich in silanol groups that are readily deprotonated in water, tyipcally giving silica a negative surface charge. The surface density of silanol groups is about 4.6/nm^2 (Bergna, 1994). Silica sols exhibit an increasingly negative electric potential with increasing pH above the isoelectric point, pH$_{iep} \sim 2-3$ (Healy, 1994). Particles can be rendered fluorescent by incorporating a silanized dye, such as fluorescein isothiocyanate (FITC) that has been treated with (3-amino-propyl)triethoxysilane (APS), during the particle synthesis (van Blaaderen and Vrij, 1992).

Like latex particles, the surface chemistry of silica can also be altered by physical adsorption of polymers and proteins, but a common modification is to render the particles organophilic by an esterification reaction with stearyl alcohol according to R. K. Iler's method (Iler, 1979; Van Helden *et al.*, 1981).

Alkoxides of other metals, including titania, can be used as precursors in the Stöber synthesis. The alkoxide reaction can also be used to coat silica onto these and other particles to create core-shell particles for optical trapping, for instance (Viravathana and Marr, 2000).

Other particle chemistries

Microrheology is not limited to the use of polystryrene or silica particles. Any colloidal particle that satisfies the criteria of probe microrheology— larger than the material microstructure, uniform in size and shape, and stably dispersable in the material of interest— can be used. Melamine resin (urea formaldehyde) is a thermosetting plastic that remains stable without swelling or degrading in a variety of organic solvents like decalin and mixtures of decalin and cyclohexylbromide (CHB) (Meyer *et al.*, 2006). Many biological samples naturally contain various particles (*e.g.*, granules or organelles) that may be used as microrheological probes, much like Heilbrunn (1924) did nearly a century ago.

1.3.2   Probe size uniformity

Quantitative measurements of rheology using embedded probe particles requires an accurate knowledge of the probe size. When using methods that measure the motion of an ensemble of particles, such as multiple particle tracking and light scattering, each particle should be roughly identical. Even microrheology methods like laser tracking and magnetic and optical tweezers that track the motion of individual particles generally require uniform particles, due to the difficulty of accurately determining particle sizes *in situ*. Fortunately, the methods of particle synthesis described in the previous section lead to narrow size distributions.

Particle size polydispersity can be measured directly by electron microscopy, or by the motion of the particles in a medium of known viscosity (*e.g.*, by dynamic light scattering). The average particle diameter will be taken as the *number average*,

$$\bar{d} = \frac{1}{N} \sum_i d_i, \qquad (1.47)$$

where d_i is the diameter of the ith measured particle in a sample of N particles. The standard deviation of the particle diameter will then be

$$\sigma = \left[\frac{1}{N} \sum_i (d_i - \bar{d})^2 \right]^{1/2} \qquad (1.48)$$

which is often reported in terms of the *coefficient of variation*

$$\text{C.V.} = (\sigma/\bar{d}) \times 100\%. \qquad (1.49)$$

Typical C.V. values for monodisperse particles are 1–2%.

1.3.3   Colloid stability

Our chief concern is the stability of the colloids used in a microrheology experiment, which depends critically on the interaction forces experienced between the particles. Colloidal particles interact with each other primarily through van der Waals attractions, electrostatic interactions, and steric forces due to polymers, proteins, or surfactants adsorbed or grafted to their surfaces.

Because of the inherent and ubiquitous van der Waals attractive forces between pieces of condensed matter, the lowest energy state of a colloidal dispersion is an aggregated mass that forms as particles

fall into their energy potential minima. Once aggregated, particles are difficult, if not impossible, to redisperse. Additional forces are thus required to render colloidal suspensions *kinetically* stable, by introducing potential energy barriers, typically an electrostatic or a steric repulsion, to keep the colloids apart despite the van der Waals attraction.

Unfortunately, the balance of forces that imparts kinetic stability to suspensions may be upset, leading to probe aggregation, as conditions vary. Examples of interest to microrheology include the ionic strength and pH of the samples or sample precursors, or bridging interactions by macromolecules and proteins. The microrheologist must therefore check for probe aggregation to ensure meaningful results. Aggregation is almost always immediately obvious in microrheology experiments that use microscopy, like particle tracking (Chapter 4). In Fig. 1.18, images taken using a fluorescence microscope of polystyrene show particles in a dispersed state, and two samples in which they have formed aggregates and large clumps. Such aggregation may be more difficult to discern when using light scattering techniques (Chapter 5). Most active microrheology methods use particle concentrations that are dilute enough that probe stability is less of an issue.

We will now briefly describe several typical colloidal interactions in more detail to understand conditions that might result in probe aggregation. Our treatment represents a sliver of the extensive knowledge concerning the interactions and stability of colloidal dispersions. We will introduce equations without the nuances of their assumptions or details of their derivations. For more in-depth discussions, the reader is referred to the many excellent colloid and surface chemistry texts available on the subject, including those by Russel, Saville, and Schowalter (1989), Hunter (2001), Hiemenz and Rajagopalan (1997), Adamson and Gast (1997), and Israelachvili (2011).

van der Waals forces

The van der Waals interaction is a nearly ubiquitous attractive force that arises, from a classical standpoint, due to fluctuations of electrons in a material, but it is ultimately quantum mechanical in nature. Only under special conditions is this inherent attraction minimized, such as when colloids are dispersed in a solvent having an identical index of refraction.

The van der Waals interaction potential between two spherical particles of micron-scale radius a, depends on the distance h separating the particle surfaces,
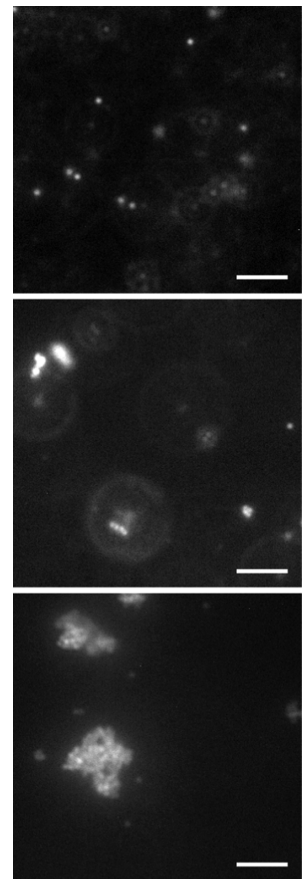
Fig. 1.18 *Fluorescence microscopy images of dispersed probe particles (top image) and samples with mild and strong aggregation. The scale bars are 10 μm.*

$$\Phi_{\text{vdw}}(h) = -\frac{A_H}{12}\left\{\left(\frac{4a^2}{4ah+h^2}\right) + \left(\frac{2a}{2a+h}\right)^2\right.$$

$$\left. +2\ln\left[1-\left(\frac{2a}{2a+h}\right)\right]\right\} \tag{1.50}$$

from which the force is calculated by $F = -d\Phi/dh$. The Hamaker constant A_H depends on the materials involved, and is typically of order 10^{-20} J for polymer particles such as polystyrene and poly(methyl methacrylate) dispersed in water, and an order of magnitude higher for metals like gold, for which $A_H \approx 3 \times 10^{-19}$ J (Hough and White, 1980).
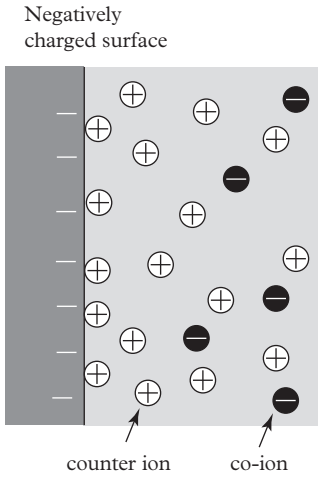
Electrostatic interactions and the electric double layer

Surface charges on colloids arise from a number of sources depending on the particle chemistry, and may include dissolution of ionic species, the dissociation of acidic sites, and the adsorption of charged species like polyelectrolytes and surfactants. These mechanisms lead to typical surface charge densities on the order of $\sigma_q = 0.005 - 0.1$ C/m^2 (often expressed in the convenient units 0.5–10 μC/cm^2) for colloidal particles of interest to microrheology. The larger of these values reflects, on average, about one charge in 1.6 nm^2.

Rather than a direct Coulombic force, charges on neighboring particle surfaces interact through a solvent, which very often contains dissolved ionic species. Ions in solution re-arrange in response to charged surfaces, forming an oppositely-charged cloud (called the *electric double layer*) that screens the surface charge. Figure 1.19 depicts an electric double-layer around a negatively-charged surface, which attracts positively-charged counter-ions, and repelling negatively charged co-ions. The distribution of charge is captured by the Gouy–Chapman model of the electric double layer, which is based on the Poisson–Boltzmann equation for the electrostatic potential $\psi(x)$ (Israelachvili, 2011). The Poisson equation

$$-\epsilon\epsilon_0\nabla^2\psi = \rho, \tag{1.51}$$

describes how a charge density ρ impacts the electrostatic potential $\psi(x)$. Here, ρ is established by the imbalance between positively- and negatively-charged ions, via

$$\rho(x) = ez\left(n_+(x) - n_-(x)\right). \tag{1.52}$$

Assuming each ion species responds to the local electrostatic potential $\psi(x)$ via the Boltzmann relation,

$$\rho = n_0 ez\left(e^{-ez\psi/k_BT} - e^{ez\psi/k_BT}\right) \tag{1.53}$$

Negatively charged surface

counter ion   co-ion

Fig. 1.19 *The diffuse double-layer near a charged interface.*

gives the Poisson–Boltzmann equation,

$$\nabla^2 \psi = \left(\frac{2zen_0}{\epsilon\epsilon_0} \right) \sinh \left(\frac{ez\psi}{k_B T} \right). \tag{1.54}$$

Further insight follows by scaling electrostatic potentials by the thermal potential

$$\psi_T = \frac{k_B T}{ze}, \tag{1.55}$$

which is roughly 26 mV at room temperature for monovalent ions, resulting in

$$\nabla^2 \tilde{\psi} = \left(\frac{2z^2 e^2 n_0}{\epsilon\epsilon_0 k_B T} \right) \sinh \tilde{\psi} \equiv \kappa^2 \sinh \tilde{\psi}, \tag{1.56}$$

where κ^{-1} is the Debye length. A more general expression, allowing for multiple ion species of various valences, is

$$\kappa^{-1} = \left(\frac{\epsilon\epsilon_0 k_B T}{\sum_i n_i e^2 z_i^2} \right)^{1/2}. \tag{1.57}$$

Detailed solutions to the Poisson–Boltzmann equation for interacting particles is beyond our current interest, but it is useful to consider at least one description of the *interparticle interaction* between charged colloids in solution. For spheres with constant potential surfaces, the double-layer interaction is (Russel *et al.*, 1989)

$$\Phi_{\text{el}}(h) = 2\pi\epsilon\epsilon_0 (k_B T/ze)^2 a\tilde{\psi}_s^2 \ln\left[1 + e^{-\kappa h} \right] \tag{1.58}$$

where $\tilde{\psi}_s = \psi_s/\psi_T$ is the scaled surface potential of the particle.

Equation 1.58 applies to conditions in which the double layer is thin relative to the particle size, $\kappa a \gg 1$, and is approximate but accurate enough for our purposes. Thin double layers form at sufficiently high-ionic strengths. Table 1.3 lists Debye lengths for the monovalent salt sodium chloride. A useful rule of thumb is $\kappa^{-1} = 0.307 \, \text{nm}/\sqrt{c_s}$ for monovalent salts, where c_s is the molar salt concentration.

The surface charge density and the type and concentration of ions in solution have the greatest effects on the double layer interactions. As we can see in Table 1.3, high-ionic strength solutions lead to a compact double layer very close to the particle surface, and comparable to the range of the van der Waals attraction. At modest ionic strengths, the Debye length is on the order of 10 nm or less. As we will

Table 1.3 *Debye lengths calculated for an aqueous solution of a monovalent salt.*

NaCl (mM)	κ^{-1} (nm)
0.1	31
1	9.7
10	3.1
100	0.97

soon show, aggregation between particles occurs as the ionic strength increases. Because the Debeye length depends on the square of the ion charge, divalent ions like Ca^{2+} and Mg^{2+} are potent inducers of aggregation. In microrheology samples, the presence of buffer salts will also contribute to double layer screening, and should be accounted for when calculating the Debye length using eqn 1.57.

It is difficult to definitively relate the surface charge density of a colloid to its electrostatic potential, or to measure the surface potential. Electrophoretic measurements of the so-called ζ-potential are often used, which reflect the potential drop across the diffuse cloud of counter-ions predicted by the Poisson–Boltzmann equation. The ζ-potential may differ from the true electrostatic potential at the surface of the colloid, which is where the colloid's surface charge density resides. Various factors are hypothesized to play key roles, including a "Stern" layer of immobilized counter-ions, possibly physically adsorbed to the surface, hydrophobic effects and water structuring around solvated ions and surfaces, and others. The difference between the electrostatic potential at the colloidal surface and the electrokinetic potential ζ depends strongly on the identity of the counter-ion, for example (Brown *et al.*, 2016).

A common approximation relating an effective colloidal surface charge density (*i.e.*, outside the Stern layer) to the electrokinetic potential ζ is given by the Graham equation,

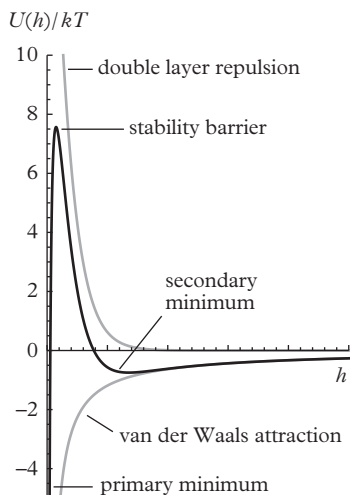$$\sigma_q = 2(2\epsilon\epsilon_0 k_B T n_b)^{1/2} \sinh \tilde{\zeta}, \qquad (1.59)$$

which follows from solutions to the nonlinear Poisson–Boltzmann equation for monovalent electrolytes. Here, n_b is the number of ions in the bulk, summed over all ion species $n_b = \sum_i n_i$.

DLVO theory

The classic theory of colloid stability is attributed to two teams of co-workers who independently derived it, Derjaguin and Landau (1941) and Verwey and Overbeek (1948). The DLVO theory combines the van der Waals and electrostatic double layer interactions described previously to calculate the total interaction potential between colloids

$$\Phi(h) = \Phi_{vdw}(h) + \Phi_{el}(h) \qquad (1.60)$$

as a function of the separation between the particle surfaces h.

An example of the DLVO potential energy is shown in Fig. 1.20. The combined van der Waals attraction and double layer repulsion

Fig. 1.20 *A schematic of the DLVO interaction potential.*

leads to three general features in the energy profile: A primary minimum, a stability barrier, and sometimes a secondary minimum. The primary minimum represents the deep, attractive energy well between two colloidal particles, set by the strong van der Waals attraction and physical repulsion at contact. The repulsive barrier at longer separations confers the kinetic stability to colloidal suspensions. Its height Φ_{max} and range sets the kinetics of aggregation between the probe particles. Two particles approach close enough to cross over the energy barrier only rarely, requiring a characteristic time scale

$$t \sim (3\pi a^3 \eta / k_B T) \exp(\Phi_{max}/k_B T). \qquad (1.61)$$

For a large stability barrier, the rate of aggregation is infinitesimal, as expected.

Depending on the range and magnitude of the double layer repulsion, a secondary minimum, beyond the range of the stability barrier, may be present. If the secondary minimum is sufficiently deep, on the order of the thermal energy $k_B T$, then particles may aggregate in this energy well. In contrast to particles that fall into the primary minimum, particles that aggregate in the secondary minimum may redisperse with a modest input of energy by weak shaking, stirring, or with the use of a mixer. Otherwise, an aggregated suspension must be subjected to a significant energy using, for instance, a probe sonicator.

Let's examine the interactions between micrometer diameter polystyrene particles at several ionic strengths of a monovalent salt (NaCl) more quantitatively. In Fig 1.21, we plot the interaction potential between particles with a surface potential of $\psi_s = -50$ mV in 1, 10, and 100 mM NaCl solutions. As illustrated in the inset, the repulsive barrier is large, on the order of several hundred $k_B T$. At low salt (1mM), the repulsive barrier extends to tens of nanometers separation. Nevertheless, a modest secondary minimum on the order of ~ 1 $k_B T$ is evident at $h = 100$ nm. At 10 mM, the secondary minimum is more pronounced, and could result in aggregation into a secondary minimum. As the NaCl concentration increases to 100 mM, the secondary minimum is now deep, and although the calculation shows a stability barrier, the separation of the barrier is on the order of nanometers. Under these conditions, the stability of the particles is likely to be compromised.

Grafted polymers and steric stabilization

Chemically grafted polymer brushes are effective stabilizers for colloids and can mitigate adsorption that leads to bridging interactions between probes, especially in protein solutions (Napper, 1983). The
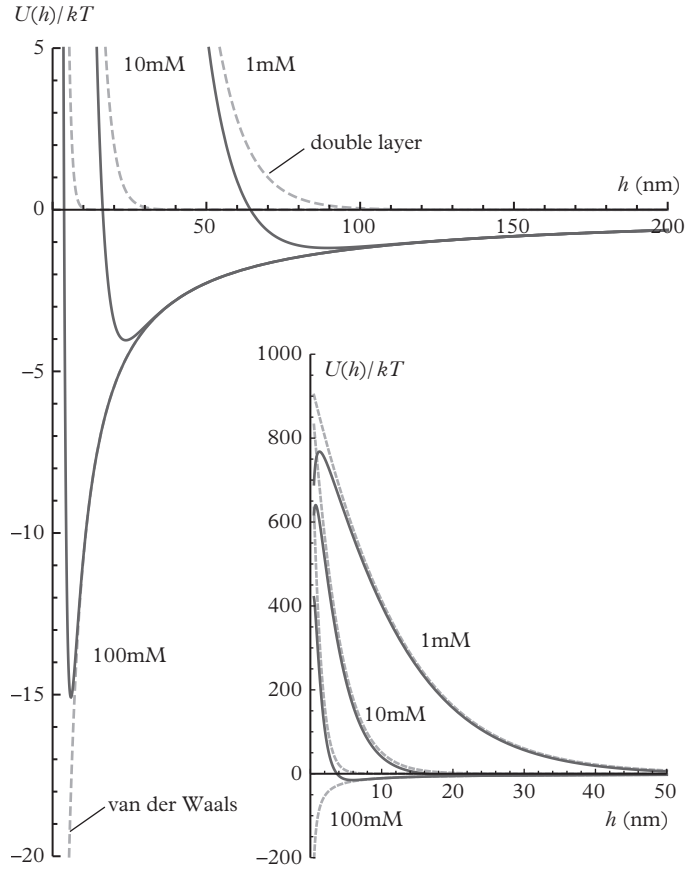
Fig. 1.21 *DLVO interaction potential as a function of surface separation h = r − 2 a calculated for 1 μm diameter polystyrene particles with a surface potential ψ_s = −50 mV in NaCl solutions from 1–100 mM. Each solid line is the total potential calculated from the sum of electrostatic double layer and van der Waals interactions. The individual contributions to the potential are indicated by dashed lines.*
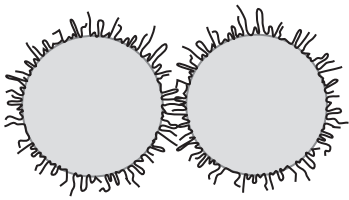
Fig. 1.22 *Grafted or adsorbed polymers produce steric interactions that can stabilize colloidal particles.*

steric repulsion produced by two adsorbed polymer layers are illustrated in Fig. 1.22. The polymer contribution to the interaction potential is

$$
\Phi_p = \begin{cases} \Phi_0 \left[-\ln y - \frac{9}{5}(1-y) + \frac{1}{3}(1-y^3) - \frac{1}{30}(1-y^6) \right], & 0 < y < 1 \\ 0 & y \geq 1 \end{cases}
\tag{1.62}
$$

where $y = h/2L = (r - 2a)/2L$ and

$$
\Phi_0 = \left(\frac{\pi L \sigma_p k_B T}{12 N_p l^2} \right) a L^2.
\tag{1.63}
$$

Here, L is the contour length, N_p is the degree of polymerization, l is the segment length, and ϕ_p is the surface graft density.

As we noted earlier, another important role for grafted polymers is to control the surface chemistry of the probes—either to tailor the interaction with the surrounding medium or to block these interactions.

Bridging interactions

When the surface concentration of adsorbed polymers or proteins is low, it is possible for molecules on one particle to stick simultaneously to a bare patch on a neighboring particle, as illustrated in Fig. 1.23. Such phenomena are called bridging interactions (Evans and Napper, 1973; de Gennes, 1987; Dickinson and Eriksson, 1991) and they represent another potential destabilization mechanism in microrheology experiments. The adsorbed material acts as a bridge that causes coagulation of the probes (Healy and LaMer, 1962; de Gennes, 1982).

Bridging interactions are normally mitigated through the use of surface chemistries that prevent or minimize adsorption, like the PEG chemistries discussed in Section 1.3.1 for polystryene probes. Competing adsorption, by pre-treating probes with protein solutions of bovine serum albumin for instance, can block the surface and provide adequate colloidal stability, but in turn may affect the probe-material interaction, as was reported for BSA-coated polystyrene probes in entangled dispersions of F-actin (McGrath *et al.*, 2000).
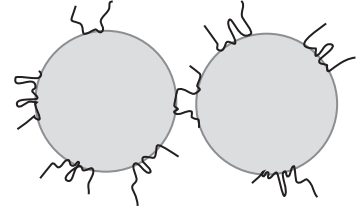
Depletion interactions

Related to steric stabilization and bridging interactions are depletion interactions (Lekkerkerker and Tuinier, 2011). In this case, the depletion attraction occurs when larger particles like probes are dispersed in a solution of a smaller non-adsorbing species, such as polymer coils, surfactant micelles, or small particles. Depletion interactions occur as larger particles come together and provide more free volume for the smaller particles (Asakura and Oosawa, 1954). An equivalent view, illustrated in Fig. 1.24, is that an osmotic pressure imbalance occurs on the large particles when they are at a separation that excludes the smaller species. The osmotic pressure of the small particles, polymer coils, or proteins, pushes the larger particles together.

The depletion interaction is calculated to a first order by considering the osmotic pressure for ideal particles with radius R_g

$$\Pi = nk_BT \qquad (1.64)$$

where n is the number density $n = \left(\frac{4}{3}\pi R_g^3\right)^{-1}$. Integrating this osmotic pressure over the available surface area of the larger particles,

Fig. 1.23 *Bridging interactions caused by adsorbed polymer or protein can destablize colloidal particles.*
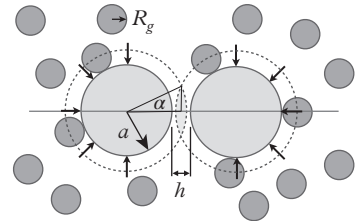
Fig. 1.24 *An osmotic pressure imbalance of the depletion interaction occurs when the excluded volume of the larger particles, indicated by the dashed lines, overlaps. The overlapping volume is highlighted and defines the angle* α.

$$F = -2\pi a^2 n k_B T \int_0^\alpha \cos\phi \sin\phi \, d\phi, \qquad (1.65)$$

with a range of angles given geometrically,

$$\cos\alpha = \frac{a + h/2}{a + R_g}, \qquad (1.66)$$

leads to

$$\frac{F}{\pi a^2 n k_B T} = \left[\left(\frac{1 + h'\Delta/2}{1 + \Delta} \right)^2 - 1 \right] \qquad (1.67)$$

with

$$\Delta = R_g / a \qquad (1.68)$$

$$h' = h/R_g. \qquad (1.69)$$

From the force, the dimensionless depletion potential is

$$\Phi' = \frac{-\Delta(h' - 2)^2 [6 + \Delta(h' + 4)]}{12(\Delta + 1)^2} \qquad (1.70)$$

where $\Phi' = \Phi/\pi a^2 R_g n k_B T$. The range of the attraction is the diameter of the depletant $2R_g$ and the attraction at particle contact can reach several to tens of $k_B T$.

1.3.4   Probe sedimentation, washing, and concentration

Having reviewed the chemistry and stability of colloidal particles, here we will make a few comments on practical issues of their use, including a short discussion of probe sedimentation, the preparation of probes by washing, and aspects related to probe concentration.

Probe sedimentation

The buoyant force exerted on a colloid is

$$F_b = \frac{4}{3}\pi a^3 \Delta\rho g \qquad (1.71)$$

where $\Delta\rho = \rho_m - \rho_p$ is the density difference between the medium and the particle, and g is the acceleration due to gravity. The sedimentation velocity of a colloid in a viscous Newtonian fluid is

$$V_b = \frac{2a^2 \Delta\rho g}{9\eta} \qquad (1.72)$$

where the hydrodynamic drag exerted on the particle is $F_d = 6\pi a \eta V_p$. For a complex, viscoelastic fluid, η is the zero shear viscosity.

The sedimentation Peclet number Pe_s is a dimensionless quantity that characterizes the magnitude of sedimentation. It is the ratio of the characteristic time scale of a particle to diffuse its radius, $a^2/D_s = 6\pi a^3 \eta / k_B T$, with respect to the characteristic time scale to sediment the same distance, a/V_s,

$$\text{Pe}_s = \frac{2\pi a^4 \Delta \rho g}{3 k_B T}. \tag{1.73}$$

Sedimentation becomes significantly stronger as the particle size increases. The sedimentation Peclet number for a 1 μm diameter polystyrene probe particle in water is about $\text{Pe}_s = 0.03$. Probe particles that are just twice this size exhibit values of $\text{Pe}_s \sim O(1)$.

Probe washing

Surfactants are often added by manufacturers to colloidal suspensions to stabilize them and improve their shelf life. Common non-ionic surfactants include Tween-20 (a polysorbate surfactant) and Tergitol (a secondary alcohol ethoxylate). Anionic surfactants like sodium dodecyl sulfate are also common stabilizers. Surfactants can potentially alter the sample through complexation or change the interactions of the probe particles with the material, and should be removed by washing the probe particles before use.

The preferred method of washing is by multiple centrifugation and redispersion steps. The probe suspension is centrifuged to form a loose pellet of particles and the supernatant pipetted off. The probes are redispersed and the process repeated three to five times. Because the surfactants confer stability, the centrifugation must be performed lightly to prevent probes from aggregating. Other methods, such as dialysis and mixing particles with an ion exchange resin, can also be used.

Probe concentration

The concentration of probe particles depends on the method of microrheology being used. In passive microrheology, the particle concentration, given by the volume fraction ϕ, will vary between 10^{-2} for experiments that employ diffusing wave spectroscopy (light scattering in the highly multiple scattering regime, which is discussed in Chapter 5) and 10^{-4} for particle tracking microrheology (see Chapter 4). Obviously, it is important that the probe particles do not influence the rheology being measured. For particles dispersed

in a Newtonian medium with viscosity η_0, Einstein showed that the viscosity of the suspension changes as the particle volume fraction increases by

$$\eta/\eta_0 = 1 + \frac{5}{2}\phi + O(\phi^2), \qquad (1.74)$$

which is valid below about $\phi < 0.05$.

Einstein's formula (and suspension viscosity formulae more general) reflect the viscosity of the suspension, as would be measured with a macroscopic rheometer. The (tracer) diffusivity of a spherical particle in a dilute suspension of identical particles, on the other hand, was computed by Batchelor (1976) and Rallison and Hinch (1976) to be

$$D_s^0 \sim D_0(1 - 1.81\phi) \qquad (1.75)$$

for short times, and

$$D_s^\infty \sim D_0(1 - 2.06\phi) \qquad (1.76)$$

for long times. As will be seen shortly, the (tracer) self-diffusivity is what is measured in many microrheology measurements to extract material rheology. In Newtonian liquids, finite probe concentrations, if not properly accounted for, would appear to give an apparent viscosity between $(1 - 1.8\phi)^{-1}$ and $(1 - 1.2\phi)^{-1}$ too high, and with a weakly non-Newtonian character.

Finite probe concentrations thus change several aspects: They directly affect the actual, macroscopically-measurable rheology of the material (by Einstein's correction in the dilute limit), as well as the self-diffusivity of each probe. Probe concentrations should therefore be as low as is feasible.

....

EXERCISES

(1.1) **Sedimentation.** A tracer particle microrheology experiment uses 1 μm polystyrene probe particles dispersed in a fluid with viscosity $\eta = 1.1 \times 10^{-3}$ Pa $\cdot$ s.

  (a) What is the sedimentation Peclet nuber?

  (b) If the sample chamber is 200 μm thick, calculate the time required for the probe particles to sediment to the bottom wall.

(c) The image plane for the experiment is positioned half-way between the sample walls. Assuming that the probe volume fraction is initially $\phi = 10^{-5}$ and that the particles are initially evenly distributed through the chamber, calculate the probe concentration in the image plane with time.

(1.2) **Probe stability.** A tracer particle microrheology experiment uses 1 μm polystyrene probe particles dispersed in a fluid with viscosity $\eta = 1.1 \times 10^{-3}$ Pa · s. Calculate the DLVO interaction potential between these particles for a surface charge density $\sigma_q = -3 \ \mu$C/cm^2 in 10 μM, 1 mM, and 100 mM aqueous NaCl solutions. Are the particles stable under these conditions?